CrossMark

ORIGINAL ARTICLE

Realization of a biomechanical model-assisted image guidance system for breast cancer surgery using supine MRI

Rebekah H. Conley[1] · Ingrid M. Meszoely[2] · Jared A. Weis[1] ·
Thomas S. Pheiffer[1] · Lori R. Arlinghaus[3] · Thomas E. Yankeelov[1,3,4,5] ·
Michael I. Miga[1,4,6]

Abstract

Purpose Unfortunately, the current re-excision rates for breast conserving surgeries due to positive margins average 20–40 %. The high re-excision rates arise from difficulty in localizing tumor boundaries intraoperatively and lack of real-time information on the presence of residual disease. The work presented here introduces the use of supine magnetic resonance (MR) images, digitization technology, and biomechanical models to investigate the capability of using an image guidance system to localize tumors intraoperatively.

Methods Preoperative supine MR images were used to create patient-specific biomechanical models of the breast tissue, chest wall, and tumor. In a mock intraoperative setup, a laser range scanner was used to digitize the breast surface and tracked ultrasound was used to digitize the chest wall and tumor. Rigid registration combined with a novel nonrigid registration routine was used to align the preoperative and intraoperative patient breast and tumor. The registra-tion framework is driven by breast surface data (laser range scan of visible surface), ultrasound chest wall surface, and MR-visible fiducials. Tumor localizations by tracked ultra-sound were *only* used to evaluate the fidelity of aligning preoperative MR tumor contours to physical patient space. The use of tracked ultrasound to digitize subsurface fea-tures to constrain our nonrigid registration approach and to assess the fidelity of our framework makes this work unique. Two patient subjects were analyzed as a preliminary inves-tigation toward the realization of this supine image-guided approach.

Results An initial rigid registration was performed using adhesive MR-visible fiducial markers for two patients sched-uled for a lumpectomy. For patient 1, the rigid registration resulted in a root-mean-square fiducial registration error (FRE) of 7.5 mm and the difference between the intraop-erative tumor centroid as visualized with tracked ultrasound imaging and the registered preoperative MR counterpart was 6.5 mm. Nonrigid correction resulted in a decrease in FRE to 2.9 mm and tumor centroid difference to 5.5 mm. For patient 2, rigid registration resulted in a FRE of 8.8 mm and a 3D tumor centroid difference of 12.5 mm. Following nonrigid correction for patient 2, the FRE was reduced to 7.4 mm and the 3D tumor centroid difference was reduced to 5.3 mm.

Conclusion Using our prototype image-guided surgery platform, we were able to align intraoperative data with preoperative patient-specific models with clinically relevant accuracy; i.e., tumor centroid localizations of approximately 5.3–5.5 mm.

✉ Rebekah H. Conley
  rebekah.h.conley@vanderbilt.edu;
  rebekah.h.conley@vanderbilt.com

1 Department of Biomedical Engineering,
  Vanderbilt University, Nashville, TN, USA

2 Department of Surgical Oncology, Vanderbilt University
  Medical Center, Nashville, TN, USA

3 Vanderbilt University Institute of Imaging Science, Nashville,
  TN, USA

4 Department of Radiology and Radiological Sciences,
  Vanderbilt University, Nashville, TN, USA

5 Departments of Physics and Cancer Biology,
  Vanderbilt University, Nashville, TN, USA

6 Department of Neurological Surgery, Vanderbilt University,
 Nashville, TN, USA

Springer

Introduction

Breast cancer is the most frequently diagnosed cancer in women and is also the leading cause of cancer-related deaths among women worldwide, with 1.7 million new cases being diagnosed and more than 500,000 deaths occurring in 2012 [15]. Breast cancer treatment is dependent upon multimodal therapy with surgery being a primary component, especially for early-stage cancers. Mastectomy (total removal of the breast) was the most common procedure choice for newly diagnosed breast cancer patients until the 1980s when studies revealed that lumpectomy, the far less disfiguring option, was shown to have the same 10-year survival rate as mastectomy [12]. Despite this fact, approximately 25–50 % of patients eligible for breast conservation therapy (BCT) will choose mastectomy over lumpectomy [1,11]. A substantial concern of BCT patients is whether or not negative margins will be obtained in the initial surgery. Negative margins are achieved when no cancer cells are present on or near (usually within 5–10 mm) the border of the excised tissue and are considered necessary for a successful lumpectomy. Unfortunately, the current re-excision rates due to positive margins average 20–40 % and range from 5 to 70 % [16]. Failure to achieve negative margins can result in the delay of radiation treatment, increase risk of local recurrence, cause psychological and physical stress on the patient, compromise cosmetic results, and increase cost.

The high re-excision rates arise from the difficulty in localizing tumor boundaries intraoperatively and lack of real-time information on the presence of residual disease [23]. The challenge in determining surgical margins intraoperatively is that geometric and spatial cues are quickly lost in the surgical presentation. Equally confounding is that valuable diagnostic images are acquired in a significantly different breast presentation than the typical surgical setup. Diagnostic and biopsy information is driven by mammography and preoperative MR images in which the patient is standing or lying prone with pendant breasts, while surgical presentation is in the supine position. An example of this challenge is displayed in Fig. 1, where the breast undergoes significant shape change between the prone and supine positions causing the tumor to deform and change location.

Current localization strategies used in the operating room (OR) include intraoperative ultrasound, wire-guided approaches, and radio-guided occult lesion localization. Prospective studies report that wire guide localization results in positive margins in 38–43 % of patients undergoing BCT [3,28]. Intraoperative ultrasound (iUS) has been shown to improve BCT [9]. However, iUS is limited by the fact that only 50 % of nonpalpable tumors are visible by ultrasound in the breast [23]. The shortcomings of radio-guided occult lesion localization are that the radioisotope must be accurately placed into the tumor and diffusion of the radiotracer into surrounding tissue decreases accuracy of the tumor location [23].

Due to the current limitations of intraoperative tumor localization approaches, the efficacy of using MR data alignment strategies has been investigated but challenges in surgical presentation have been identified. There is little doubt that the use of MR data to influence surgical planning has important implications in the surgical management of patients [5,6]. We believe that better image-to-physical data alignment strategies can be used more directly for better surgical management. To achieve this, methods using biomechanical models for prone-to-supine registration of MR images have been suggested [7,14]. Recently, utilization of supine MR images for surgical guidance has been considered in frameworks for image-guided breast surgery [2,8,25].
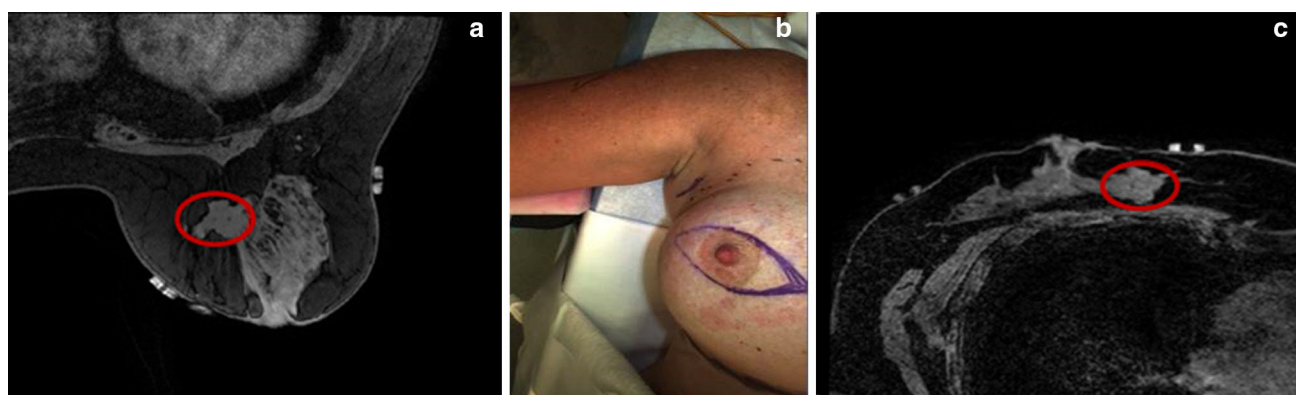
Fig. 1 Demonstration of the challenge of using preoperative images for surgical guidance. **a** and **c** are axial slices of T_1-weighted THRIVE sequence MR images in the prone and supine positions with *red ovals* designating the same tumor in the same axial slice. Changes in patient setup cause the tumor to move, yielding the diagnostic scan in (**a**) less valuable for locating the tumor in the surgical setup, shown in (**b**). **a** Prone MR image of breast. **b** OR presentation. **c** Supine MR image of breast

Alignment of presurgical supine MR images to surgically oriented MR images using surface markers has also been shown to be feasible [10]. Preoperative supine MR images registered using surface markers coupled with an intraoperative optical scan of the breast have also demonstrated qualitative alignment value [20]. While encouraging, the integration of supine MR images, optical tracking and digitization technology, patient-specific biomechanical models for nonrigid registration, and tracked ultrasound for subsurface feature localization has yet to be realized as a surgical guidance platform for breast conserving surgery. This paper integrates these components and reports preliminary experiences with this surgical platform in two patient cases. In addition, subsurface target accuracy is assessed indepen-

dently using tracked ultrasound imaging of echogenic tumors in both cases.

Methods

Two breast cancer patients scheduled for surgery were selected in a Vanderbilt IRB approved bystander study with informed consent to evaluate the feasibility and accuracy of our image guidance platform. In Fig. 2, a schematic overview demonstrates the structure of the proposed system with required data inputs and generalized outputs at each step. While our guidance platform does not require ultrasound-visible tumors, their visibility in B-mode ultrasound images
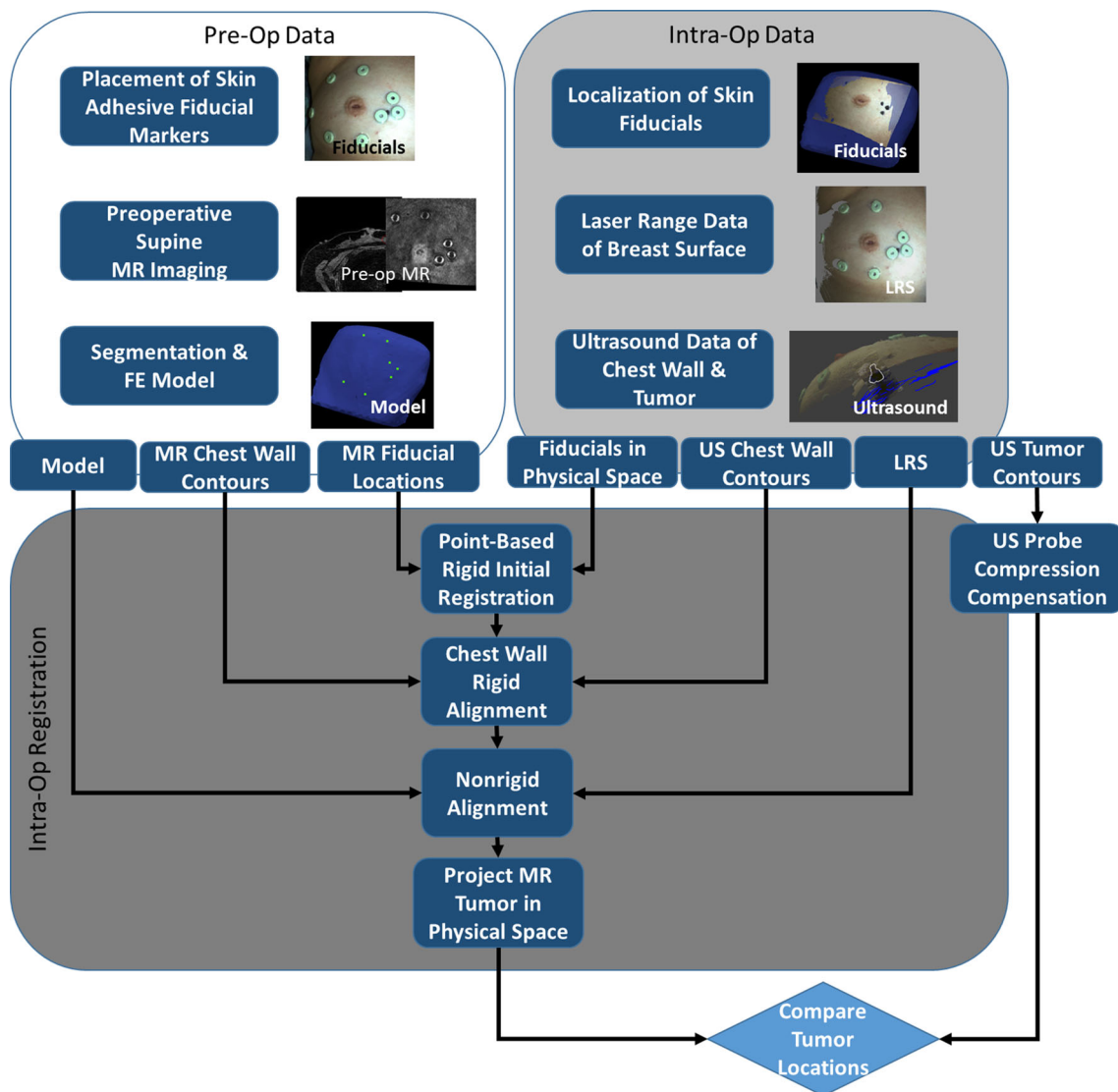
Fig. 2 Overview of surgical guidance platform and validation framework. The preoperative (preOp) and intraoperative (intraOp) data panels summarize the important information gathered at each step. This information is then systematically incorporated into an intraOP registration framework. The final outcome is a preoperative tumor mapped to physical space which can then be quantitatively compared to the location of the tumor in the OR

in this study was particularly useful for evaluating the subsurface alignment accuracy of our registration approach.

Preoperative data collection

Supine MR imaging

Preoperative supine MR images were acquired for each patient and were used to create patient-specific biomechanical models of the breast tissue, chest wall, and tumor. MR-visible adhesive skin fiducial markers (IZI Medical Products, Owing Mills, MD) were placed over ink markings distributed across the breast surface. The patient was carefully positioned in a closed bore 3T Achieva MR scanner (Philips Healthcare, Best, the Netherlands). A 16-channel sensitivity encoding (SENSE) torso coil was situated carefully as to not deform the breast, and the ipsilateral arm was placed above the patient's head to more closely replicate surgical presentation. High-resolution anatomical images were acquired with a T_1-weighted, 3D turbo field echo sequence with fat suppression, a field of view of $200 \times 200 \times 160 \, \text{mm}^3$, and a reconstructed

voxel size of $0.391 \times 0.391 \times 1 \, \text{mm}^3$. Recently, we have achieved successful acquisitions of contrast-enhanced supine images, an example of a contrast-enhanced image volume of a patient volunteer is shown in Fig. 3. For the patient subjects studied herein, tumors were identified from the diagnostic MR supine images and were segmented semi-automatically.

Patient-specific model

The supine image volume from each patient was segmented into breast tissue, tumor, and chest wall (pectoral muscle) using a semi-automatic segmentation technique by Insight Registration and Segmentation Toolkit (ITK)-SNAP [29]. Figure 4a illustrates the segmentation step for patient 1. The locations of the synthetic fiducial center points were manually determined and recorded (Fig. 4b). Following segmentation, a binary mask of the whole breast was used to generate an isosurface using a standard marching cubes algorithm [17]. The isosurface was then smoothed with a radial basis function using FastRBF Toolbox (Farfield Technologies, Christchurch, New England). From this surface, a finite
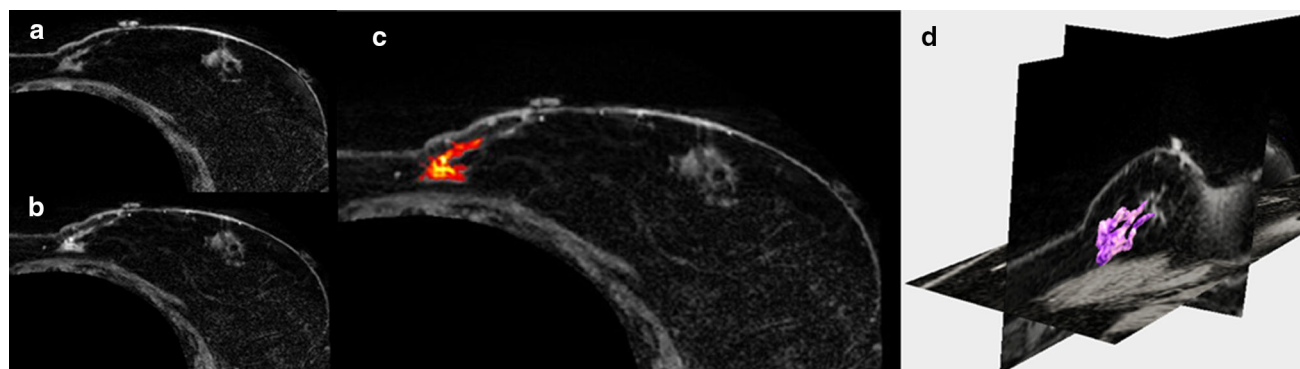
Fig. 3 Axial slices of supine MRI of patient volunteer with **a** precontrast, **b** post-contrast injection, **c** contrast-enhanced tumor, and **d** 3D segmentation of tumor (*magenta*)
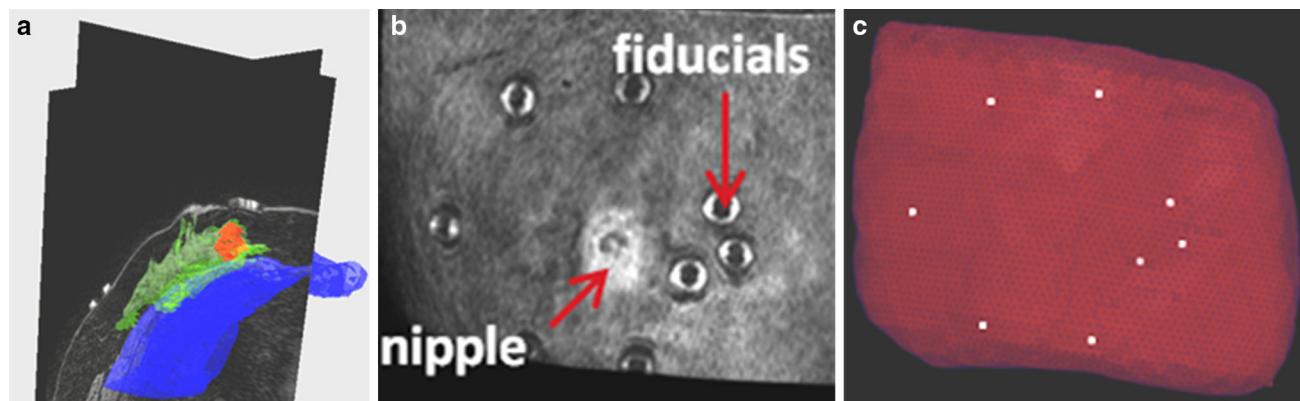
Fig. 4 Segmentation of preoperative supine MR images: **a** segmentation of glandular tissue in *green*, chest wall in *blue*, and tumor in *red*. **b** is a volume render of the supine MR image, **c** preoperative mesh showing location of fiducial centers in *white*
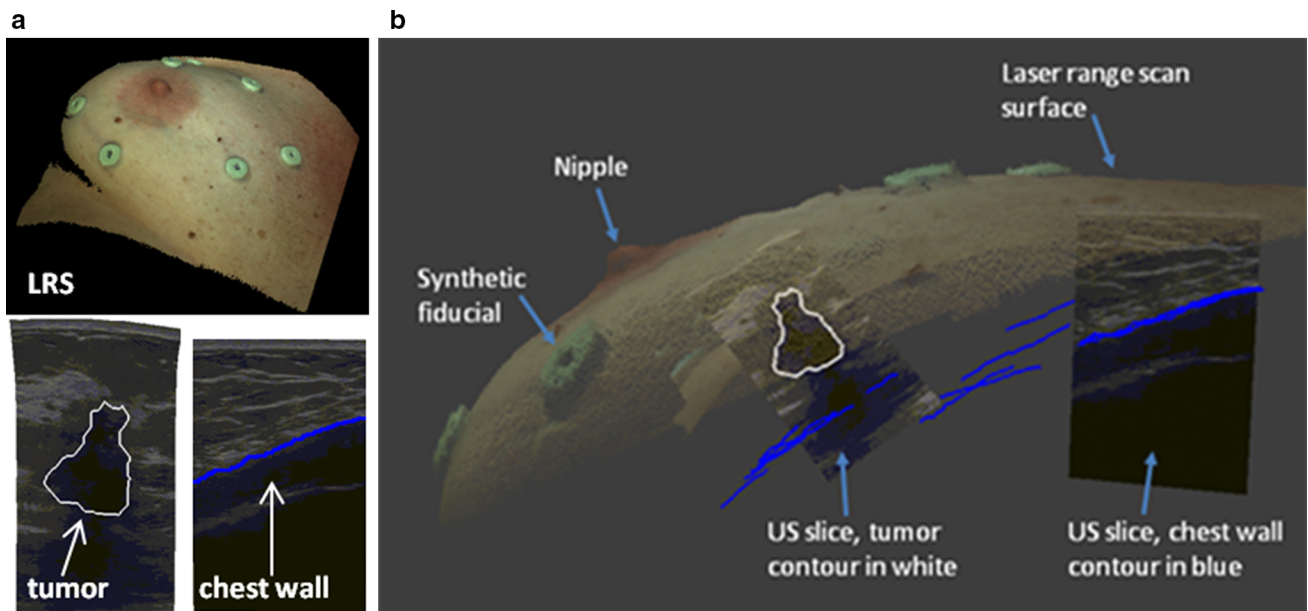
Fig. 5 a *Top* LRS scan of patient 2 breast. *Bottom left* compression corrected ultrasound image with tumor contour in *white*. *Bottom right* ultrasound image with chest wall contour in *blue*. **b** Fusion display of tracked intraoperative data containing a textured point cloud, adhesive fiducial markers, tracked ultrasound images, tumor contour (*white*), and chest wall contours (*blue*)

element tetrahedral mesh was generated using a custom mesh generator [27] with a mesh edge-length resolution of approximately 3 mm (Fig. 4c).

Mock intraoperative data collection

As an initial investigation, a mock intraoperative setup to collect simulated intraoperative data was performed for each patient. In this study, mock intraoperative data were collected to avoid workflow disruptions in the OR and were analyzed on the same day as preoperative imaging to minimize patient volunteer time. The true intraoperative scenario would involve intraoperative data, such as that shown in Fig. 5, to be collected during surgery. To address realistic patient conditions in the mock setup, positioning was performed by a surgical oncologist [IMM], to accurately depict OR positioning. Once complete, skin fiducials are digitized with an optical stylus, laser range data are acquired, and an ultrasound examination is performed. In the following subsections, the extent of this data and its integration is explained.

Surface and feature digitization

A custom-built, optically tracked laser range scanner (Pathfinder Technologies, Inc, Nashville, TN, USA) was used to digitize the breast surface by sweeping a laser line over the breast surface and recording geometric points along with color information of the visible field (Fig. 5a top, b), yielding a textured point cloud with known 3D coordinates in physical space. The physical space points corresponding to the MR-visible fiducial center points are determined by the black ink markings that were placed on the patient's skin prior to adhering the MR-visible fiducials. An optically tracked stylus was used to collect the location of the ink markings. The textured point cloud was used to confirm the location of the fiducial points by comparing the coordinates collected by the tracked stylus with the field of view color texture information collected from the laser range scanner. All geometric measurements were made with a Polaris Spectra (Northern Digital, Waterloo, ON, Canada) optical tracking system.

Ultrasound exam

The ultrasound portion of this study was performed in two parts: (1) target B-mode imaging of tumor and (2) chest wall swabbing. Figure 5a bottom left, bottom right shows representative contours of each, respectively. Ultrasound images were acquired using an Acuson Antares ultrasound machine (Siemens, Munich, Germany) using a VFX13-5 linear array probe set at 10 MHz. The depth was set at 6 cm to maintain visibility of the chest wall throughout the examination. A passive optically tracked rigid body was attached to the ultrasound transducer. The tracked ultrasound was calibrated using the method developed by Muratore et al. [19] that takes multiple B-mode ultrasound images of a tracked stylus tip in the imaging plane to develop a rigid transformation between the image plane and physical space. Once calibrated,
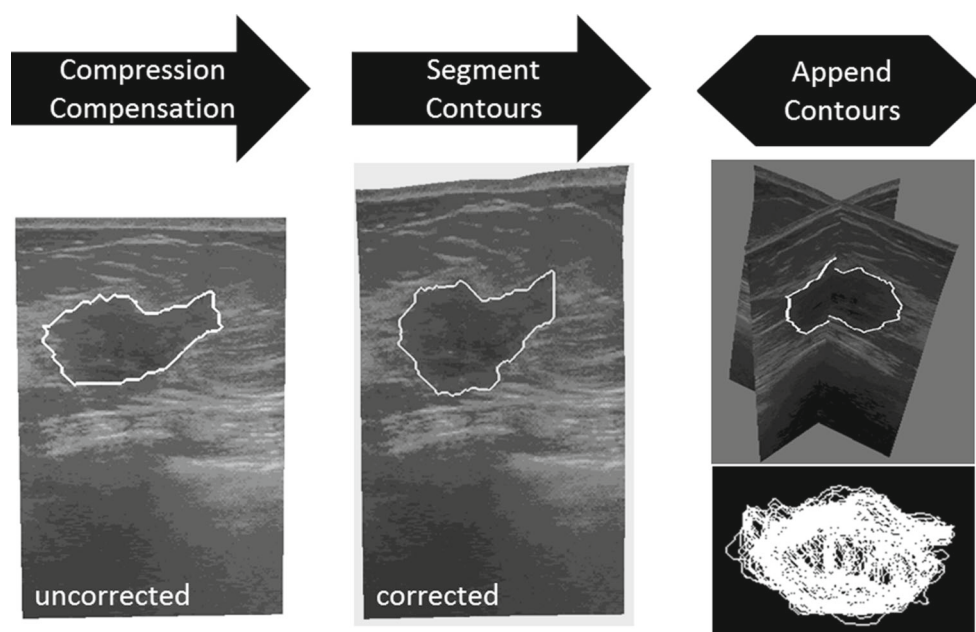
Fig. 6 Steps involved in processing tracked intraoperative ultrasound data. The ultrasound images are first corrected for tissue compression exerted by the ultrasound transducer. The tumor contour is then seg-mented in each 2D slice. Lastly, all contours are appended to form a 3D representation of the intraoperative tumor

all pixels in the ultrasound plane have a corresponding 3D coordinate in physical space.

In addition to optical tracking for determining the location of ultrasound-visualized structures, it is also important to correct the localization data of structures that are affected by ultrasound probe compression, namely the tumor (chest wall was assumed rigid). More specifically, since preoperative supine MR images are acquired without this compression, a correction scheme to account for deformation induced by the probe itself is needed in all ultrasound images of the echogenic tumor. Reported in [22], the fidelity of the method we utilized demonstrated reduced subsurface localization errors due to ultrasound probe compression by 67.8 and 51.6 % in phantom and clinical experiments, respectively. For the work reported in this study, it was particularly important to utilize these methods as tumor localization was serving as the primary means for accuracy evaluation of our platform.

Figure 6 provides a visual overview of the processing steps involved in acquiring tracked ultrasound data of the intraoperative tumor volume. Tumor borders are semi-automatically segmented using a custom implementation of the Livewire technique [18]. The acquired tumor ultrasound image/contour is then corrected for probe deformation and each is appended, yielding a 3D point cloud set. Similar steps are performed for the chest wall but probe deformation compensation is not necessary. Figure 5b shows a comprehensive representation of all digitization data rendered consistently within physical space: textured point cloud, synthetic fiducial landmarks, and tracked ultrasound images of

both probe-corrected tumor and chest wall ultrasound slices with segmented contours.

Registration method

The entirety of our registration approach is captured in Fig. 7. Briefly described, an initial rigid alignment is performed using the synthetic fiducials adhered to the breast. Once complete, a series of steps is conducted to estimate the influence of gravity-induced and ipsilateral arm position changes between supine imaging and surgical configurations. The influence of these variables is realized as a gravitational inducing body force and boundary conditions which are applied to a biomechanical model of the breast. Once complete, the combined rigid and nonrigid transformation provides a means to map preoperative tumor locations into physical space which can then be subsequently compared to a separate independent ultrasound-identified tumor localization.

Rigid alignment

An initial rigid alignment was performed by registering the MR-digitized marker locations to their intraoperative counterparts using a traditional 3D point-based singular value decomposition registration algorithm [26]. The point-based registration algorithm finds the optimal translation and rotation to minimize the fiducial registration error (FRE) as defined by:
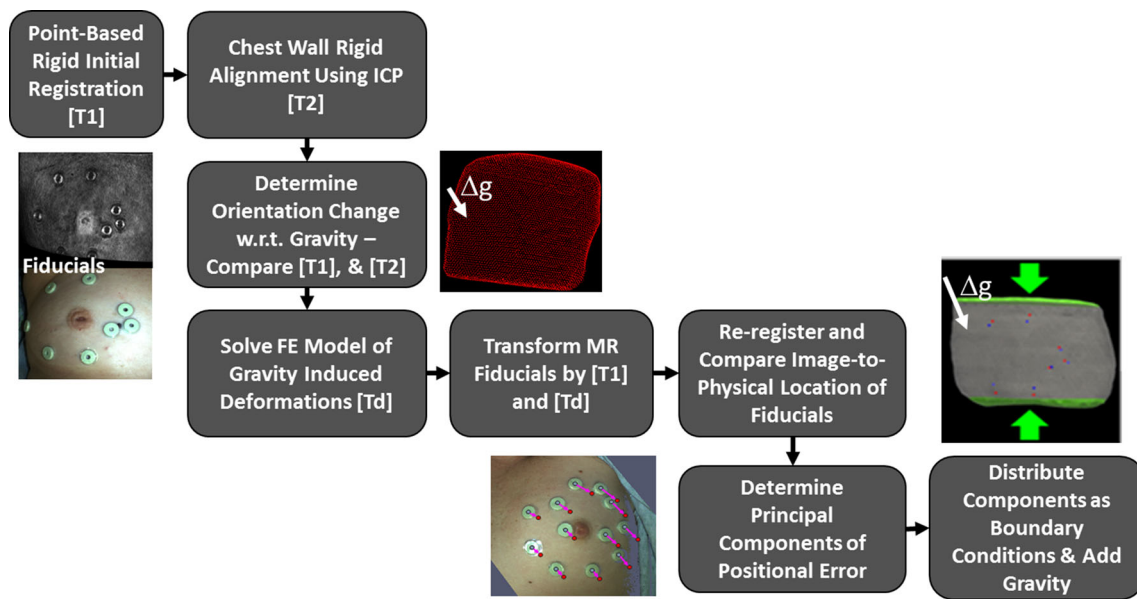
Fig. 7 Overview of the registration process beginning with rigid initialization and concluding with full nonrigid model compensation

$$\text{FRE} = \sqrt{\frac{1}{N}\sum_{i=1}^{N}(R(x_i + \Delta x_i)) + t - (y_i + \Delta y_i)} \qquad (1)$$

where x_i and y_i are 3×1 vectors of corresponding points in two spaces, Δx_i and Δy_i are the fiducial localization errors for each point in the two spaces, N is the total number of fiducials, R is a 3×3 rotation matrix, and t is a 3×1 vector containing displacements. The resulting translation vector and rotation matrix are applied to the preoperative data to provide an initial alignment with the intraoperative space.

Quantification of gravity-induced deformations

Based on initial studies investigating the use of point-based registration of skin fiducials, it was found that significant rotation of the breast occurs relative to the chest wall between supine imaging and intraoperative presentation in some cases. This results in a body force-based deformation whereby the breast becomes free to move under the influence of gravity. To estimate this change, we have elected a novel strategy. The chest wall is designated from the preoperative supine images during our breast model building process ("Patient specific model"). In addition, chest wall contours are also identified and segmented from our tracked ultrasound examination ("Ultrasound exam"). Using the fiducial-based registration ("Rigid alignment") as an initial configuration, a traditional iterative closest point (ICP) registration [4] was employed between the transformed preoperative chest wall points and the intraoperative chest wall contours as digitized by tracked iUS. The rotation matrix resulting from the ICP registration is applied to the intraoperative gravity vector

(assumed to be in the direction normal to the patient's bed). Details of this approach are outlined in Algorithm 1.

Algorithm 1 Algorithm for finding gravity-induced deformations using ICP registration

1. Initialize by transforming preoperative chest wall contours to intraoperative space using transformation from "Rigid alignment"
2. Perform an ICP registration between MR chest wall surface and iUS chest wall contours
3. Extract the rotation matrix from the final transformation and apply to the gravity vector in intraoperative space

$$\Delta g = R * g_{intraop} \qquad (2)$$

where $g_{intraop}$ is a 3×1 vector containing the unit direction normal to the patient bed in intraoperative space

---

Mechanics-based nonrigid correction

Deformations due to gravity-induced changes derived from Algorithm 1 and tissue migration of the breast due to ipsilateral arm movement are estimated using a 3D linear elastic model. The model employs the Navier–Cauchy equations and generates a displacement field for correction and is shown here:

$$\nabla \cdot (G\nabla u) + \nabla\left(\frac{G}{1-2v}(\nabla \cdot u)\right) + \rho(\Delta g) = 0 \qquad (3)$$

where v is Poisson's ratio, G is the shear modulus of elasticity ($G = E \, / \, 2(1 + v)$), u is the 3D displacement vector, ρ is the tissue density, and Δg is the change in gravitational

acceleration constant with respect to imaging and surgical presentations. Equation 3 was solved using the Galerkin Method of Weighted Residuals with linear Lagrange polynomials defined locally on the tetrahedral elements as the supporting basis and weighting functions. Solving this system results in displacement vectors defined at each node that satisfy static equilibrium conditions. The displacements are then applied to deform the preoperative mesh. In this work, an elastic modulus (E) of 1 kPa, tissue density of $1000\,\mathrm{kg/m^3}$, and Poisson's ratio of 0.485 were applied for the whole breast volume.

First model solve—application of gravity-induced deformations

Gravity-induced deformations were simulated by supplying the elastic model with a body force of tissue weight based on the change in acting gravity direction as determined in Sect. "Quantification of gravity-induced deformations". We again assume that the chest wall is a rigid fixed structure. Therefore, the boundary conditions applied to this model solve imposed fixed chest wall nodes (zero displacement) with stress-free boundary conditions elsewhere. The displacements generated from this model solve were applied to the preoperative mesh and used to estimate the remaining positional error of fiducial targets.

Final model solve

Nonrigid deformations of the breast due to ipsilateral arm movement were accounted for by applying Dirichlet boundary conditions at control surfaces along the inferior–superior surfaces of the model mesh based on preoperative imaging data. The nodes corresponding to the interior chest wall and the medial breast surface were fixed. The medial breast face was fixed because negligible movement occurs in the vicinity of the patient's sternum. The remainder of the breast surface, i.e., the visible breast during presentation, was designated as stress free.

The locations, direction, and magnitude of the applied Dirichlet boundary conditions for the inferior–superior surfaces were determined by analyzing the misalignment between the co-registered surface fiducials after gravity-induced changes were taken into account. In both patient cases, a reduced stretching of the breast between preoperative and intraoperative states was observed and used to determine model displacement boundary conditions at the inferior–superior surfaces. This reduced stretching phenomenon is shown in Fig. 8a, c, where the preoperative intra-fiducial distances (red arrows) are larger than the intraoperative intra-fiducial distances (blue arrows). One relatively simple approach to correction is to perform a principal component analysis (PCA) on the difference vector between the

co-registered fiducial points to determine the direction in which the largest deformation has occurred. PCA is performed after the displacement field from the first model solve ("1st model solve- application of gravity-induced deformations") has been applied to the preoperative FE mesh and re-registered using the new locations of the preoperative fiducials. The largest distance vector between the gravity-transformed preoperative and intraoperative intra-fiducial locations was used to approximate the magnitude of stretching/compression. Being consistent with a simple deployment strategy, the approximated displacement application was then distributed evenly among two control surfaces, as can be seen in Fig. 8b, d. The proposed registration method requires only two model solves, providing a fast correction strategy that can be readily adapted in the operating room. Given the nature of breast deformation and the reduced domain of the breast analyzed, this initial realization is purposefully designed to be work-flow friendly, operationally robust, and constrained to establish a baseline understanding of efficacy. In the discussion below, avenues for improvement are suggested.

Registration assessment

Surface markers were used to quantify registration accuracy by calculating the root-mean-square fiducial registration error (FRE). FRE is a measure of overall misalignment between fiducials and captures fiducial localization errors as well as nonrigid movements. It is important to note that fiducial location differences between image and physical space were not used as direct displacement boundary conditions in the model, but only as a measure of fit with respect to applied deformations from gravity-induced changes and inferior–superior control surfaces. With respect to subsurface targeting accuracy, tracked ultrasound image contours of the tumor were compared to their registered preoperative counterpart. More specifically, the centroid location of the preoperative segmented tumor is mapped by the process shown in Fig. 7 and compared to the centroid location of the appended 3D tracked iUS tumor contours as shown in Fig. 6. The Euclidean distance ($l_2 - norm$) between the intraoperative tumor centroid ($C_{intraop}$) and preoperative tumor centroid (C_{preop}) was used to measure target registration error: Centroid Difference = $||C_{intraop} - C_{preop}||$.

Results

Patient 1

The initial rigid alignment of the synthetic skin fiducials for patient 1 yielded an FRE 7.5 mm. Figure 9a–c shows results from the rigid registration. The tumor centroid difference between the mapped preoperative and intraoperative
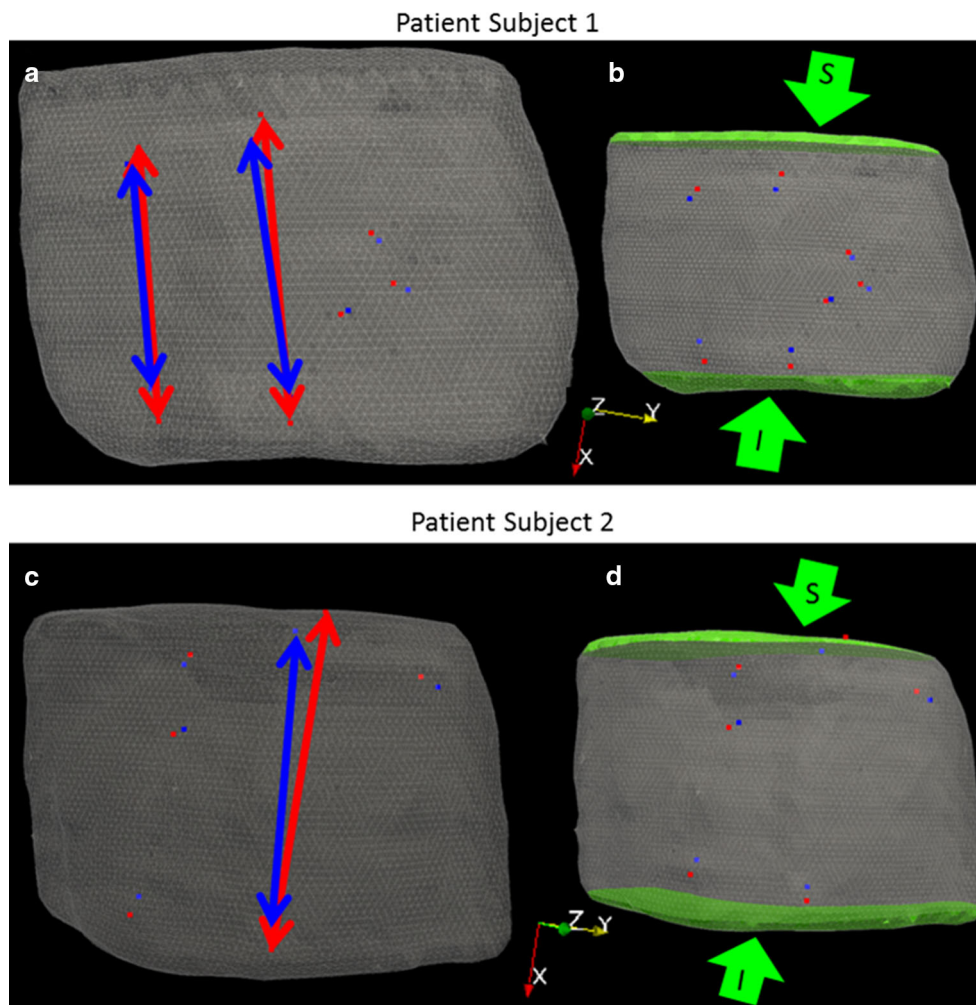
Fig. 8 **a**, **c** Preoperative mesh with *arrows* showing preoperative (*red*) and intraoperative (*blue*) intra-fiducial distances, **b**, **d** *Green arrows* point to direction of applied boundary conditions to inferior (*I*) and superior (*S*) breast faces highlighted in *green*

states before ultrasound probe compression correction of the intraoperative tumor was 7.5 mm. After probe-to-tissue compression compensation, the tumor centroid difference was 6.5 mm. The iterative closest point registration of the intraoperative and preoperative chest walls revealed that negligible rotation of the torso occurred for patient 1. Therefore, a gravitation body force was not applied. Principal component analysis of the difference in preoperative and intraoperative fiducial locations revealed a vector supporting approximately 20 mm maximum intra-fiducial distance which its largest component reflective of deformation was along the inferior–superior axis. The difference in intra-fiducial distances can be visualized in Fig. 8a, where the red arrows point to preoperative fiducials and blue arrows point to intraoperative fiducials. This maximum intra-fiducial distance difference was distributed evenly among the two control surfaces. A 10-mm displacement vector was applied to each node on the inferior and superior breast surfaces (green surface shown in Fig. 8b). The green arrows in Fig. 8b show the direction of the applied

displacements. Using these boundary conditions to drive the elastic model, the nonrigid corrected FRE was 2.9 mm and the deformation-corrected tumor centroid difference was 5.5 mm. In Fig. 9d, we can observe the improved alignment between the MR-rendered tumor and an ultrasound-visible counterpart (white contour) for patient 1.

Patient 2

Initial rigid alignment of the synthetic skin fiducials for patient subject 2 returned an FRE of 8.8 mm. Figure 9e–g shows results from the rigid registration. The tumor centroid distance between mapped preoperative and intraoperative states before ultrasound compression compensation of the tumor contours was 14.7 mm. The tumor centroid distance after probe-to-tissue compensation was 12.5 mm. Following gravitational direction correction, the FRE improved negligibly to 8.5 mm and with a more considerable correction to the tumor centroid distance decreasing to 8.4 mm. As
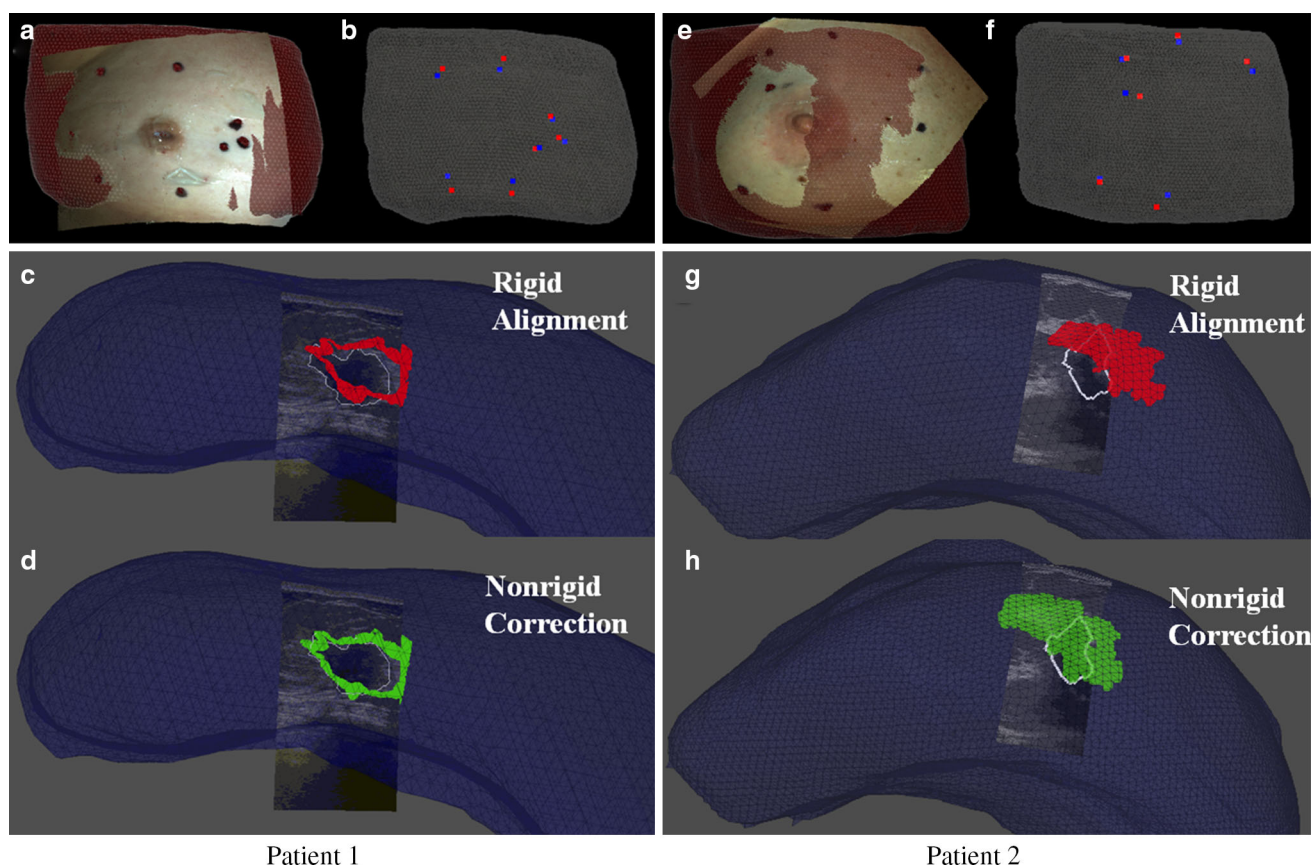
Fig. 9 Patient 1 (**a–d**) and Patient 2 (**e–h**). **a, e** Co-registered textured point cloud and preoperative mesh. **b, f** Co-registered preoperative fiducials (*red*) and intraoperative fiducials (*blue*). **c, g** Intraoperative ultrasound image with white tumor contour overlaid on preoperative rigid aligned tumors in *red*. **d, h** Intraoperative ultrasound image with white tumor contour overlaid on preoperative nonrigid corrected tumors in *green*

anticipated, principal component analysis following gravity-induced deformation compensation revealed that the largest deformations occurred along the patient's inferior–superior axis. The largest difference in the intra-fiducial distances was 50 mm. Red and blue arrows in Fig. 8c show the largest difference in preoperative and intraoperative intra-fiducial distances, respectively. The maximum intra-fiducial distance difference was distributed evenly among the two control surfaces. The green arrows in Fig. 8d point to the direction of applied displacement boundary conditions with a 25 mm displacement applied at each breast face (highlighted green surface in Fig. 8d). The nonrigid correction resulted in an FRE of 7.4 mm and tumor centroid distance of 5.4 mm. In Fig. 9h, we can observe the improved alignment between MR-rendered tumor and the ultrasound-visible counterpart (white contour) for patient 2.

Discussion

We have presented two patient subjects as an initial investigation toward the realization of a supine image-guided surgical platform. In general, the results show that initial rigid alignments are not sufficient and a nonrigid correction is necessary to obtain a clinically relevant image-to-physical alignment. In each case, arm movement between the preoperative and intraoperative patient setups caused a change in stretch to the breast tissue along the patient's inferior–superior axis. Tissue deformation exerted by the ultrasound probe required correction to improve the fidelity of using tracked ultrasound images of the tumor as a means to assess subsurface target registration error. In this study, a somewhat "open-loop," i.e., noniterative, correction strategy was used in that an initial fiducial registration error was analyzed, body forces and boundary condition were derived, a model was executed, and finally a nonrigid correction was provided. While arguably a coarse nonrigid deformation correction approach, the results are encouraging and speak to the promise of supine image-guided breast surgery. In the future, an iterative optimization strategy will be developed to find the best correction possible driven by all of the information available intraoperatively. Options for additional data already exist. The corrections shown in Fig. 9 are driven by synthetic fiducial error. This is an admittedly sparse source of data to drive the correc-

tion process and other possibilities exist in our approach. For example, while not used in this work, the laser range data shown in Fig. 5 could serve within a shape conformity metric and be employed as a constraint to the nonrigid registration framework.

Several sources of error may contribute to the reported registration inaccuracy. The tracking error of our system has been reported as sub-millimetric for passively tracked rigid stylus bodies [13]. However, multiple reference targets were attached on range-based targeting devices (laser range scanner and ultrasound). Our tracked laser range scanner has been characterized previously at 2.2 ± 1.0 mm [21] although its use in this particular work was minimal. With respect to the tracked ultrasound imaging, in studies not reported here, we have found our average target registration error to be 1.5–2.5 mm in typical tracking experiments [22]. It is difficult to predict how these errors will combine due to the nature of the registration process. More specifically, our registration approach samples both far-field (chest wall) and near-field (synthetic fiducials) structures which likely constrains internal target error; more study is needed.

Other sources of error between MR-localized fiducial and co-localized ink markings in physical space could be present. While some compensation for iUS error was performed, the validation metrics themselves still have some error. The contour digitization of the tumor using tracked ultrasound may not represent a comprehensive digitization of tumor volume and as a result could produce discrepancies of the tumor volume centroid as compared to its preoperative counterpart. In this study, care was taken to acquire ultrasound images of the tumor in orthogonal planes and at multiple angles to best digitize the whole tumor volume. Despite this care, it is unlikely that the measurement is as rigorous as its tomographic counterpart in MR. Another source of error is our use of a linear elastic model for the nonrigid correction of breast tissue. While small-strain approximations are likely violated, we have found linear models to behave reasonably well in such gross nonrigid alignment procedures. In other work [24], we have compared linear and nonlinear approaches (linear vs co-rotational finite element approaches) with similar registration problems. The observed differences between these models usually have been quite modest when compared to gross misalignments and instrument error. While all of these errors need further characterization, the results in Fig. 9 are difficult to discount. In each, we see a marked improvement in alignment between ultrasound-visualized intraoperative tumor contour and the preoperative tumor.

Conclusion

The work reported herein establishes a preliminary realization of an image-guided breast surgery approach using supine MR images. A workflow friendly alignment procedure using rigid and nonrigid registration methods is proposed and preliminary data in two patients are reported. The two cases represent a reasonable extent of the configurations possible during image-guided lumpectomy with the first patient (small breast volume) not experiencing gross volumetric misalignment after rigid registration, and the second (large breast volume) showing large shifts of the subsurface tumor target. In each, our investigational correction methodology showed considerable improvement in alignment both in quantitative metrics as well as visual overlays. To our knowledge, this work represents the first comprehensive image-guided breast surgery platform using supine MR and nonrigid model-based registration methods that has been tested under appropriate in vivo clinical conditions with subsurface target registration errors being reported using echogenic tumors. The results are very encouraging at this early stage and many avenues for future work to improve guidance alignment are possible.

Conflict of interest The authors declare that they have no conflict of interest.

References

1. Adkisson CD, Bagaria SP, Parker AS, Bray JM, Gibson T, Thomas CS, Heckman MG, McLaughlin SA (2012) Which eligible breast conservation patients choose mastectomy in the setting of newly diagnosed breast cancer? Ann Surg Oncol 19(4):1129–1136

2. Alderliesten T, Loo C, Paape A, Muller S, Rutgers E, Peeters MJV, Gilhuijs K (2010) On the feasibility of mri-guided navigation to demarcate breast cancer for breast-conserving surgery. Med Phys 37(6):2617–2626

3. Allweis TM, Kaufman Z, Lelcuk S, Pappo I, Karni T, Schneebaum S, Spector R, Schindel A, Hershko D, Zilberman M, Sayfan J, Berlin Y, Hadary A, Olsha O, Paran H, Gutman M, Carmon M (2008) A prospective, randomized, controlled, multicenter study of a real-time, intraoperative probe for positive margin detection in breast-conserving surgery. Am J Surg 196(4):483–489

4. Besl PJ, McKay ND (1992) Method for registration of 3-d shapes. In: Robotics-DL tentative. International Society for Optics and Photonics, pp 586–606

5. Braun M, Pölcher M, Schrading S, Zivanovic O, Kowalski T, Flucke U, Leutner C, Park-Simon TW, Rudlowski C, Kuhn W, Kuhl CK (2008) Influence of preoperative mri on the surgical management of patients with operable breast cancer. Breast Cancer Res Treat 111(1):179–187

6. Buxant F, Scuotto F, Hottat N, Noël JC, Simon P (2007) Does preoperative magnetic resonance imaging modify breast cancer surgery? Acta chirurgica Belgica 107(3):288

7. Carter T, Tanner C, Beechey-Newman N, Barratt D, Hawkes D (2008) Mr navigated breast surgery: method and initial clinical experience. In: Medical image computing and computer-assisted intervention-MICCAI 2008. Springer, pp 356–363

8. Conley RH, Meszoely IM, Pheiffer TS, Weis JA, Yankeelov TE, Miga MI (2014) Image to physical space registration of supine breast mri for image guided breast surgery. In: SPIE Medical Imaging. International Society for Optics and Photonics, p 90362N

9. Davis KM, Hsu CH, Bouton ME, Wilhelmson KL, Komenaka IK (2011) Intraoperative ultrasound can decrease the re-excision lumpectomy rate in patients with palpable breast cancers. Am Surg 77(6):720–725

10. Ebrahimi M, Siegler P, Modhafar A, Holloway CM, Plewes DB, Martel AL (2014) Using surface markers for mri guided breast conserving surgery: a feasibility survey. Phys Med Biol 59(7):1589

11. Fancher TT, Palesty JA, Thomas R, Healy T, Fancher JM, Ng C, Dudrick SJ (2009) A woman's influence to choose mastectomy as treatment for breast cancer. J Surg Res 153(1):128–131

12. Fisher B, Bauer M, Margolese R, Poisson R, Pilch Y, Redmond C, Fisher E, Wolmark N, Deutsch M, Montague E, Saffer E, Wickerham L, Lerner H, Glass A, Shibata H, Deckers P, Ketcham A, Oishi R, Russel I (1985) Five-year results of a randomized clinical trial comparing total mastectomy and segmental mastectomy with or without radiation in the treatment of breast cancer. N Engl J Med 312(11):665–673

13. Glossop ND (2009) Advantages of optical compared with electromagnetic tracking. J Bone Jt Surg 91(Supplement 1):23–28

14. Han L, Hipwell J, Eiben B, Barratt D, Modat M, Ourselin S, Hawkes D (2014) A nonlinear biomechanical model based registration method for aligning prone and supine mr breast images. Med Imaging IEEE Trans 33(3):682–694

15. Jemal A, Bray F, Center MM, Ferlay J, Ward E, Forman D (2011) Global cancer statistics. CA: Cancer J Clinicians 61(2):69–90

16. Landercasper J, Whitacre E, Degnim AC, Al-Hamadani M (2014) Reasons for re-excision after lumpectomy for breast cancer: insight from the american society of breast surgeons masterysm database. Ann Surg Oncol 21(10):3185–3191

17. Lorensen WE, Cline HE (1987) Marching cubes: a high resolution 3d surface construction algorithm. In: ACM siggraph computer graphics, vol 21. ACM, pp 163–169

18. Mortensen EN, Barrett WA (1995) Intelligent scissors for image composition. In: Proceedings of the 22nd annual conference on computer graphics and interactive techniques, pp 191–198

19. Muratore DM, Galloway RL Jr (2001) Beam calibration without a phantom for creating a 3-d freehand ultrasound system. Ultrasound Med Biol 27(11):1557–1566

20. Pallone MJ, Poplack SP, Avutu HBR, Paulsen KD, Barth Jr RJ (2014) Supine breast mri and 3d optical scanning: a novel approach to improve tumor localization for breast conserving surgery. Ann Surg Oncol 21(7):2203–2208

21. Pheiffer TS, Simpson AL, Lennon B, Thompson RC, Miga MI (2012) Design and evaluation of an optically-tracked single-ccd laser range scanner. Med Phys 39(2):636–642

22. Pheiffer TS, Thompson RC, Rucker DC, Simpson AL, Miga MI (2014) Model-based correction of tissue compression for tracked ultrasound in soft tissue image-guided surgery. Ultrasound Med Biol 40(4):788–803

23. Pleijhuis RG, Graafland M, de Vries J, Bart J, de Jong JS, van Dam GM (2009) Obtaining adequate surgical margins in breast-conserving therapy for patients with early-stage breast cancer: current modalities and future directions. Ann Surg Oncol 16(10):2717–2730

24. Rucker D, Wu Y, Clements L, Ondrake J, Pheiffer T, Simpson A, Jarnagin W, Miga M (2014) A mechanics-based nonrigid registration method for liver surgery using sparse intraoperative data. Med Imaging IEEE Trans 33(1):147–158

25. Siegler P, Holloway C, Causer P, Thevathasan G, Plewes DB (2011) Supine breast mri. J Magn Reson Imaging 34(5):1212–1217

26. Sonka M, Fitzpatrick JM (2000) Handbook of medical imaging(volume 2, medical image processing and analysis). SPIE- The International Society for Optical Engineering

27. Sullivan JM Jr, Charron G, Paulsen KD (1997) A three-dimensional mesh generator for arbitrary multiple material domains. Finite Elem Anal Des 25(3):219–241

28. Tafra L, Fine R, Whitworth P, Berry M, Woods J, Ekbom G, Gass J, Beitsch P, Dodge D, Han L, Potruch T, Francescatti D, Oetting L, Smith JS, Snider H, Kleban D, Chagpar A, Akbari S (2006) Prospective randomized study comparing cryo-assisted and needle-wire localization of ultrasound-visible breast tumors. Am J Surg 192(4):462–470

29. Yushkevich PA, Piven J, Hazlett HC, Smith RG, Ho S, Gee JC, Gerig G (2006) User-guided 3d active contour segmentation of anatomical structures: significantly improved efficiency and reliability. Neuroimage 31(3):1116–1128